A Case Study on the Impact of Moisture Variability on Convection Initiation Using Radar Refractivity Retrievals

D. BODINE

School of Meteorology, and Atmospheric Radar Research Center, University of Oklahoma, Norman, Oklahoma

P. L. HEINSELMAN

NOAA/OAR National Severe Storms Laboratory, Norman, Oklahoma

B. L. CHEONG

Atmospheric Radar Research Center, University of Oklahoma, Norman, Oklahoma

R. D. PALMER AND D. MICHAUD

School of Meteorology, and Atmospheric Radar Research Center, University of Oklahoma, Norman, Oklahoma

(Manuscript received 31 July 2009, in final form 11 March 2010)

ABSTRACT

A case study illustrating the impact of moisture variability on convection initiation in a synoptically active environment without strong moisture gradients is presented. The preconvective environment on 30 April 2007 nearly satisfied the three conditions for convection initiation: moisture, instability, and a low-level lifting mechanism. However, a sounding analysis showed that a low-level inversion layer and high LFC would prevent convection initiation because the convective updraft velocities required to overcome the convective inhibition (CIN) were much higher than updraft velocities typically observed in convergence zones. Radar refractivity retrievals from the Twin Lakes, Oklahoma (KTLX), Weather Surveillance Radar-1988 Doppler (WSR-88D) showed a moisture pool contributing up to a 2°C increase in dewpoint temperature where the initial storm-scale convergence was observed. The analysis of the storm-relative wind field revealed that the developing storm ingested the higher moisture associated with the moisture pool. Sounding analyses showed that the moisture pool reduced or nearly eliminated CIN, lowered the LFC by about 500 m, and increased CAPE by 2.5 times. Thus, these small-scale moisture changes increased the likelihood of convection initiation within the moisture pool by creating a more favorable thermodynamic environment. The results suggest that refractivity data could improve convection initiation forecasts by assessing moisture variability at finer scales than the current observation network.

1. Introduction

The absence of small-scale moisture measurements near the surface is a major limitation in forecasting convective precipitation (Emanuel et al. 1995; Dabberdt and Schlatter 1996; National Research Council 1998). Recent breakthroughs in retrieving near-surface refractivity from weather radar provide new opportunities for high-resolution, near-surface moisture measurements (Fabry et al. 1997; Fabry 2004; Cheong et al. 2008). Refractivity retrievals obtained from the Weather Surveillance Radar-1988 Doppler (WSR-88D) network can provide moisture measurements with very high spatial (as small as 2 km) and temporal resolution (4.2–10 min, depending on volume coverage pattern). However, the range coverage is limited to a 20–40-km radius around the radar. These measurements provide superior spatial resolution to the Automated Surface Observing System (ASOS), which has an average spacing of 90 km (Koch and Saleeby 2001).

Several observational and modeling studies have shown that moisture variability plays an important role in convection initiation. Deep lifting of boundary layer moisture

Corresponding author address: David Bodine, School of Meteorology, University of Oklahoma, 120 David L. Boren Blvd., Suite 5900, Norman, OK 73072.
E-mail: bodine@ou.edu

DOI: 10.1175/2010JAMC2360.1

is needed for convection initiation, often occurring along strong moisture gradients such as the dryline (Ziegler et al. 1997; Ziegler and Rasmussen 1998; Parsons et al. 2000). The Convection and Precipitation/Electrification (CaPE) project (Weckwerth et al. 1996; Weckwerth 2000) focused on the impact of moisture variability on convection initiation in a quiescent environment. During the CaPE project, Weckwerth et al. (1996) found that differences in moisture between updraft and downdraft branches of horizontal convective rolls (HCRs) ranged from 1.5 to 2.5 g kg^{-1}. The CaPE project demonstrated that HCR updraft branches could sufficiently lower the LFC and reduce the convective inhibition (CIN) to enable convection initiation through boundary layer forcing (Weckwerth 2000). Using a combination of radar refractivity data and in situ moisture measurements from aircraft obtained during the International H_20 Project (IHOP; Weckwerth et al. 2004), Fabry (2006) found that moisture variability had a greater effect on CIN than temperature variability at scales less than 20 km. On the other hand, Crook (1996) found that the CIN is more sensitive to surface temperature variations than surface moisture variations when the thermodynamic profile was modified in the numerical model. However, Crook (1996) found that convection initiation in the model was still sensitive to moisture changes as small as 1 g kg^{-1}.

Several papers have suggested potential applications for using radar refractivity retrievals to enhance short-term convection initiation forecasts (Fabry 2004; Weckwerth et al. 2005; Fabry 2006; Wakimoto and Murphey 2009). Results from IHOP revealed the capability to use refractivity data to observe moisture changes associated with cold fronts, outflow boundaries, drylines, boundary layer structures, variations in surface moisture fluxes, and nocturnal moisture boundaries (Weckwerth et al. 2005; Fabry 2006; Demoz et al. 2006; Buban et al. 2007; Roberts et al. 2008; Wakimoto and Murphey 2009). Weckwerth et al. (2005) also showed that radar refractivity data could be used to identify strengthening moisture gradients associated with a dryline before a fine line developed in reflectivity, and Roberts et al. (2008) presented a similar case where increasing moisture gradients along a convergent boundary preceded convection initiation. Though these studies have presented promising applications of radar refractivity retrievals, an operational evaluation of refractivity at the Norman, Oklahoma, Weather Forecast Office (WFO) found that the participating forecasters did not obtain significant benefits from refractivity data, and gave low importance to implementing refractivity into the Advanced Weather Interactive Processing System (AWIPS; Heinselman et al. 2009). One forecaster suggested that additional research is needed to identify new applications of refractivity data that provide new information to forecasters that cannot be obtained from the current observation network; in their case the Oklahoma Mesonet (Brock et al. 1995; McPherson et al. 2007).

The objective of this study is to demonstrate the capability to use radar refractivity data to observe small-scale moisture variability, and to investigate the impact of this moisture variability on convection initiation in a synoptically active environment. Most observational studies have focused on the impact of moisture variability on convection initiation in quiescent conditions (e.g., Weckwerth 2000), or examined convection initiation cases with strong moisture gradients associated with boundaries (e.g., drylines, outflow boundaries). In previous radar refractivity studies of convection initiation, cases showing boundaries with significant moisture gradients were presented (Weckwerth et al. 2005; Roberts et al. 2008). This study, on the other hand, investigates the impact of a small-scale moisture pool, observed only within the radar refractivity field, on convection initiation.

Section 2 briefly describes the radar refractivity algorithm developed at the Atmospheric Radar Research Center (ARRC) at the University of Oklahoma (OU), and presents a preliminary error analysis. The refractivity data and other data used in the case study are discussed in section 3. The convection initiation case study is presented in section 4. Therein, the synoptic and preconvective mesoscale environments are described, and observations of the moisture variability from radar refractivity retrievals are presented. Then, the impact of moisture variability on convection initiation is investigated through sounding analyses. Section 5 presents a summary and discussion of the results.

2. Radar refractivity retrieval algorithm

The ARRC has developed an independent algorithm for refractivity retrieval based on the work by Fabry et al. (1997). The ARRC algorithm has been adapted easily for different weather radars, including the WSR-88Ds, the Collaborative Adaptive Sensing of the Atmosphere (CASA; McLaughlin et al. 2009) X-band radars, and the National Weather Radar Testbed (NWRT) phased array radar (PAR; Zrnić et al. 2007). Cheong et al. (2008) provide a detailed description of the ARRC algorithm, although it is briefly described here for completeness.

The refractive index, n, is often rewritten in terms of refractivity, N, to improve the ease of interpretation (Bean and Dutton 1968):

$$N = (n - 1) \times 10^6. \quad (1)$$

Bean and Dutton (1968) showed that refractivity could be related to temperature, pressure, and water vapor pressure using the following equation:

$$N = 77.6\frac{p}{T} + 3.73 \times 10^5 \frac{e}{T^2}, \quad (2)$$

where p is pressure in hectopascals, T is the temperature in kelvins, and e is the water vapor pressure in hectopascals. At warmer temperatures, refractivity provides a good approximation for surface moisture, as temperature and pressure changes affect refractivity less than moisture changes (see Fig. 2 of Fabry et al. 1997).

Radar refractivity retrievals are obtained using phase measurements between the radar and ground clutter targets. Reference phase measurements are made when the moisture field is nearly homogeneous and constant with time. At the same time, an objectively analyzed refractivity field is derived from Oklahoma Mesonet (Mesonet, hereinafter) data (Brock et al. 1995; McPherson et al. 2007) to create a reference refractivity field. Radar refractivity is computed from Mesonet relative humidity, temperature, and pressure measurements, which have 5-min temporal resolution and 35-km spatial resolution. Real-time phase measurements are collected to produce a phase difference field using the reference and real-time phase measurements. Poor clutter targets are then censored based on clutter quality indices. The resulting phase difference field is relatively noisy and sparse, so the phase difference field is smoothed using a 2.5-km Gaussian window. Next, the radial derivative of the phase difference field is computed to obtain the refractivity change field. The resulting refractivity change field is subsequently smoothed to reduce the noise introduced by the derivative operation. Absolute refractivity (hereafter, refractivity) can be computed by adding the refractivity change and the reference refractivity fields. Scan-to-scan refractivity change (hereinafter, scan-to-scan refractivity) is computed by substituting the phase measurements from the previous scan for the reference phase measurements, and applying the same procedure to the phase difference data.

A preliminary error analysis was conducted on the KTLX (Twin Lakes, Oklahoma; Fig. 1) WSR-88D refractivity data to evaluate the accuracy of refractivity data derived from the ARRC algorithm. The refractivity data used for this error analysis were collected between 22 April and 8 May 2007, during the KTLX Spring 2007 Refractivity Experiment (Heinselman et al. 2009). Refractivity data flow was interrupted between 2054 UTC 2 May 2007 and 1408 UTC 3 May 2007. Because the Norman, Oklahoma (NRMN; Fig. 1), Mesonet station is located within good radar refractivity coverage, the KTLX-derived refractivity field is compared with the NRMN observed refractivity field. The time series plot (Fig. 2) shows good agreement between the radar and NRMN refractivity measurements, even during rapidly changing conditions (e.g., advancing and retreating drylines on 22–23 April 2007). The correlation coefficient between the Mesonet and radar refractivity measurements was 0.976, showing excellent correlation between the two measurements.

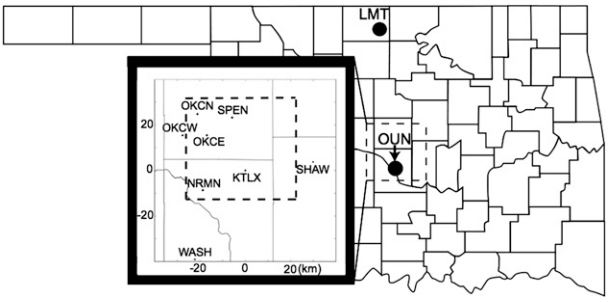

FIG. 1. Plot showing the location of the sounding sites (OUN and LMT), KTLX, and Mesonet stations. The dashed box shows the approximate region of the KTLX refractivity domain, and large inset box shows the Mesonet stations within the domain. The dashed box inside the large inset box shows the region highlighted in Fig. 4.

The refractivity bias ϵ^i was computed from refractivity and NRMN Mesonet refractivity data using the following equation,

$$\epsilon^i = N^i_{\text{refrac}} - N^i_{\text{NRMN}}, \quad (3)$$

where N^i_{refrac} and N^i_{NRMN} are the refractivity and NRMN Mesonet refractivity measurements at time i, respectively. The mean bias was -4.2 N units for the period from 22 April to 8 May 2007. Even after removing the mean bias, the root-mean-squared error was 3.2 N units, primarily the result of the time-varying bias. We suspect the time-varying bias is related to changes in the near-surface, vertical refractivity gradient. As a result, a time-varying bias often occurs in the early morning hours during periods of anomalous propagation. Other possible sources of radar refractivity bias include vegetation sway, severe anomalous propagation, precipitation, and frequency drift (Fabry 2004). Refractivity gradients and scan-to-scan refractivity, less affected by the time-varying bias than refractivity, are the two primary fields used in this study. The ARRC is currently studying this bias problem and developing mitigation schemes.

3. Data

Radar, sounding, and Mesonet data (introduced in section 2) were used to assess the synoptic and mesoscale environments and analyze the thermodynamic environment before and during convection initiation. The

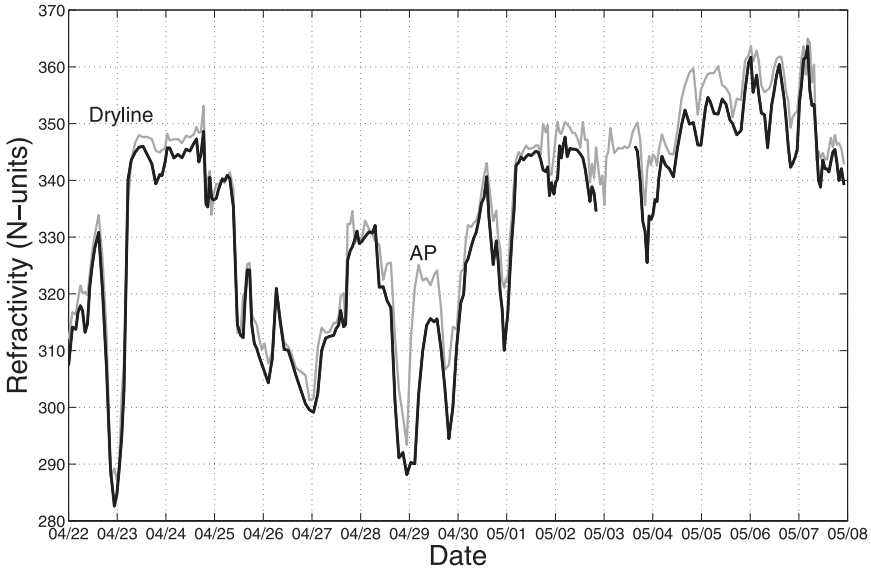

FIG. 2. Time series plot of radar refractivity (black line) and the Norman Mesonet-derived refractivity (light gray line) between 22 Apr and 8 May 2007. The time series plot shows excellent correlation between the Mesonet and radar refractivity measurements, even during rapidly evolving conditions such as an advancing and retreating dryline on 22–23 Apr 2007. A large bias often occurs in the early morning hours, possibly caused by anomalous propagation (AP). Radar refractivity data flow was interrupted between 2054 UTC 2 and 1408 UTC 3 May 2007.

locations of the radar, sounding sites, and Mesonet stations used in this study are shown in Fig. 1.

Four radar products from the KTLX WSR-88D were obtained for 1723–1816 UTC 30 April 2007: Level-II reflectivity and radial velocity, Level-III velocity azimuth display (VAD), and refractivity data. KTLX was operating in clear-air mode between 1723 and 1811 UTC, and was switched to precipitation mode thereafter.

Plan-position indicator (PPI) plots were generated using the Warning Decision Support System—Integrated Information (WDSSII; Lakshmanan et al. 2006, 2007). The reflectivity and radial velocity data were gridded to Cartesian coordinates, along the specified elevation angle, using radar beam geometry as described by Lakshmanan et al. (2006). Storm motion and divergence were calculated from these gridded data. The WDSSII display was used to compute storm motion (Lakshmanan et al. 2007). Divergence δ was computed from the radial velocity v_r of two range gates, n and $n + k$, within the same azimuth angle, using

$$\delta = \frac{v_r^{n+k} - v_r^n}{\Delta r}. \quad (4)$$

The distance between range gates $n + k$ and n is given by Δr, which was 1 km for this study.

Radiosonde data and Rapid Update Cycle (RUC; Benjamin et al. 2004) analyses were obtained to diagnose the preconvective synoptic and mesoscale environments. Radiosonde data from Norman (OUN; Fig. 1) were used to analyze the thermodynamic profile, and modified using the Skew-*T*/Hodograph Analysis Research Program (NSHARP; Hart and Korotky 1991) to study the effects of moisture changes on the thermodynamic environment. Data from the Lamont, Oklahoma (LMT; Fig. 1), sounding were also used for comparison. RUC analyses were examined to identify synoptically favorable regions for convection initiation.

4. The 30 April 2007 case study

An isolated storm with reflectivity as high as 66 dB*Z* developed near Oklahoma City, Oklahoma, shortly after 1800 UTC 30 April 2007. This section presents an overview of the synoptic and mesoscale environment, a discussion of the ingredients in convection initiation, and an investigation of the impact of moisture variability on convection initiation.

a. Synoptic and mesoscale environment

The 1800 UTC 30 April 2007 RUC analysis showed that the convection initiation region (central Oklahoma) was situated between the 500-hPa shortwave trough axis located over western Texas and the 500-hPa shortwave ridge axis over southern Missouri and Arkansas (Fig. 3a). A 500-hPa cutoff low was centered over eastern New

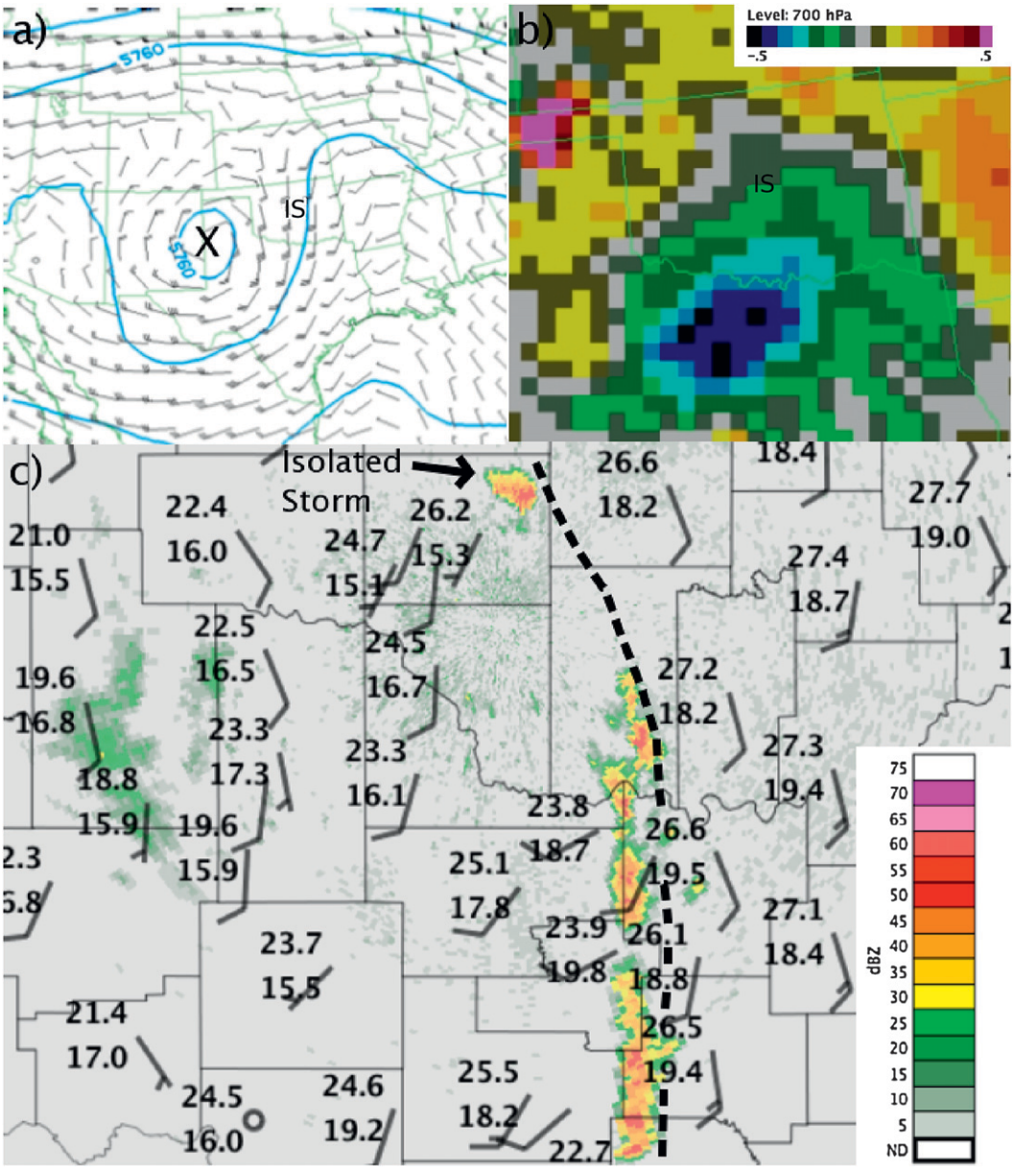

FIG. 3. Plots from 30 Apr 2007 showing the (a) RUC 500-hPa analysis at 1800 UTC, (b) RUC 700-hPa vertical velocity field (Pa s^{-1}) at 1800 UTC, and (c) surface and radar observations at 1825 UTC. The 500-hPa geopotential heights are contoured in solid blue lines at 60-m intervals, and wind barbs (m s^{-1}) showing wind speed and direction are plotted. The half barb and full barb represent a 2.5 and 5 m s^{-1} wind speed, respectively. The black X denotes the vorticity maximum at 500 hPa. Mesonet temperature (°C), dewpoint temperature (°C), 10-m wind barb (m s^{-1}), and 0.5°-tilt reflectivity at 1825 UTC are plotted in the surface analysis. The black dashed line demarcates the mesoscale boundary, and the black arrow points to the developing isolated storm.

Mexico and the Texas Panhandle, and was collocated with a maximum in 500-hPa absolute vorticity (Fig. 3a). The region downstream from the cutoff low was favorable for upward motion at lower and midlevels owing to increasing positive vorticity advection between 850 and 500 hPa (not shown). The 1800 UTC RUC 700-hPa analysis revealed weak upward motion between −0.05 and −0.1 Pa s^{-1} over central Oklahoma (Fig. 3b), further suggesting that the region was favorable for synoptic-scale ascent.

The surface analysis from 1825 UTC showed a mesoscale boundary (MB), characterized by a weak temperature gradient (Fig. 3c). The source of the MB appeared to be a weak cold pool from ongoing precipitation in

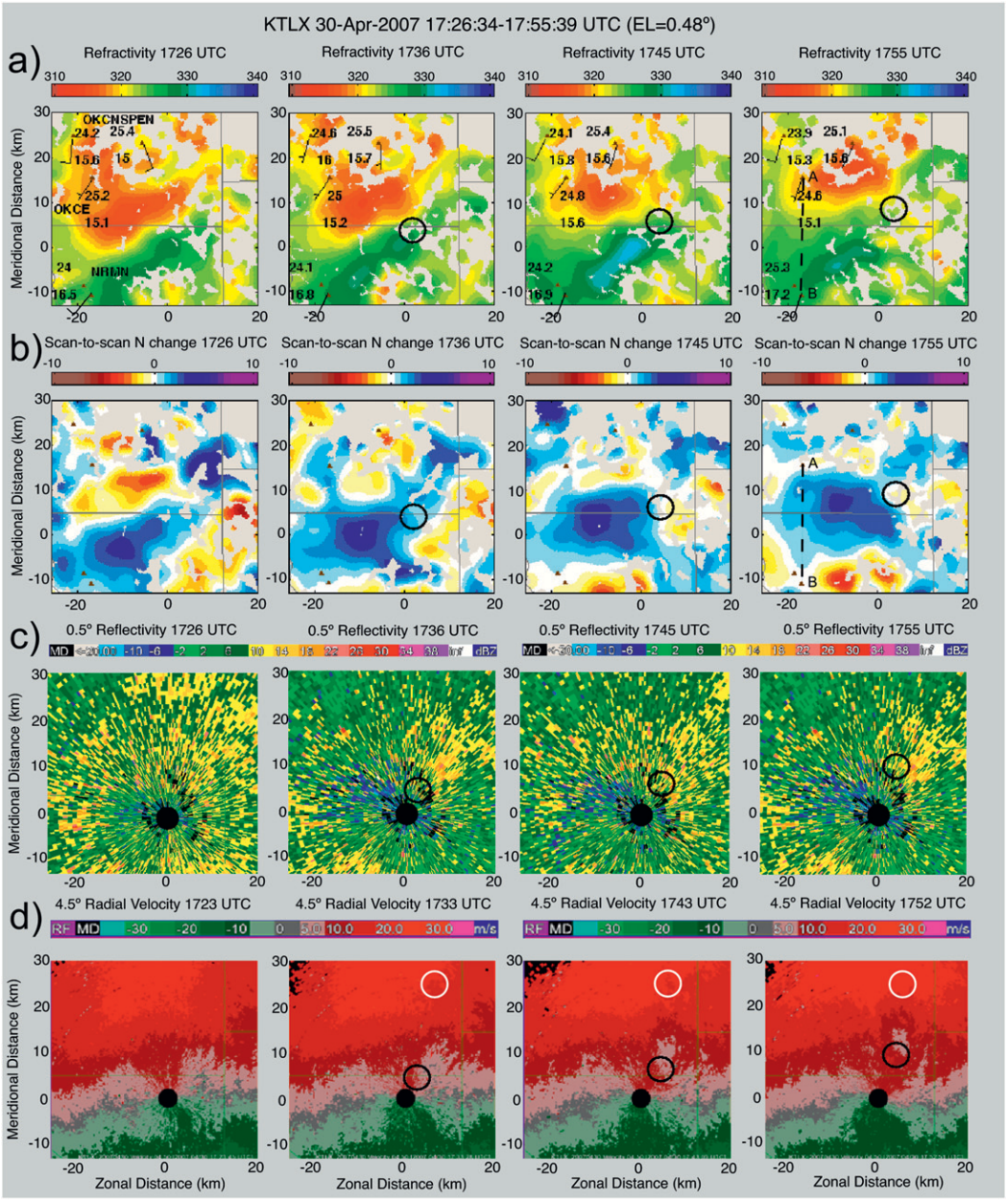

FIG. 4. (a) Refractivity, (b) scan-to-scan refractivity, and (c) 0.5°-tilt reflectivity at 1726, 1736, 1745, and 1755 UTC 30 Apr 2007, and (d) 4.5°-tilt radial velocity at 1723, 1733, 1743, and 1752 UTC 30 Apr 2007. The black circles on each field mark the location of the convergent signature in radial velocity associated with the updraft, and the white circles on (d) show the location of convection initiation. Mesonet temperature, dewpoint temperature, and wind barbs (same as Fig. 3) are plotted on the refractivity panels. The filled black circles in (c) and (d) show the radar location. On the velocity scale, RF indicates range folding and MD indicates missing data.

southwest Oklahoma. The surface analysis showed the MB extending southward from central Oklahoma, with southwesterly winds west of the MB and southerly winds east of the MB (Fig. 3c). Small dewpoint temperature differences across the MB of up to 2°–3°C were also observed. At 1825 UTC, a line of convection had developed along the MB in southern Oklahoma, and an isolated convective cell formed along the MB near Oklahoma City (Fig. 3c).

During the hour prior to convection initiation of the isolated convective cell, significant moisture variability was observed in the refractivity (Fig. 4a) and scan-to-scan

refractivity (Fig. 4b) fields in the area where the isolated convective cell developed. The moisture pool was most clearly depicted by scan-to-scan refractivity, which showed a region of positive scan-to-scan refractivity moving north-northeast at approximately 5 m s^{-1} (Fig. 4b). At 1755 UTC, the radar refractivity difference across the moisture pool was 10 N units, and the corresponding difference in dewpoint temperature from the Mesonet was 2°C between Oklahoma City East (OKCE; point A in Figs. 4a,b) and NRMN (point B in Figs. 4a,b) Mesonet stations. Assuming constant temperature and pressure, the 2°C change in dewpoint temperature measured between these stations was equal to a 10 N-unit change in refractivity, showing good agreement between the Mesonet and radar refractivity observations. The reflectivity and radial velocity field relative to the moisture pool is discussed later (Figs. 4c,d). The left edge of the moisture pool passed over the NRMN and OKCE Mesonet stations and produced a small change in dewpoint temperature. At 1811 UTC, the northern edge of the moisture pool was 3 km south of the Spencer, Oklahoma (SPEN), Mesonet station (Fig. 5a,b). Given the northward movement of the moisture pool at 5 m s^{-1} or 18 km h^{-1}, the moisture pool likely arrived at about 1820 UTC. This calculation is supported by the corresponding moisture increase observed at SPEN between 1820 and 1845 UTC, when the dewpoint temperature rose from 14.8° to 16.2°C (Fig. 6a), and the radar refractivity increased 5 N units (Fig. 6b).

Although the lower and midlevel dynamics were favorable for synoptic-scale ascent, a mesoscale mechanism for low-level lift was necessary for convection initiation (e.g., Doswell 1987). The Mesonet data showed the MB, which indicated mesoscale, low-level lift along the MB. A fine line was observed within the MB (Fig. 5c), indicating increased convergence along the MB and an enhanced low-level mesoscale lifting mechanism necessary for convection initiation. The moisture pool (Figs. 5a,b) was located west of the north–south-oriented fine line seen in the 0.5°-tilt reflectivity field at 1805 and 1815 UTC (Fig. 5c). Once the fine line developed, it showed temporal continuity between scans, enhanced reflectivity at lower tilts, and cross-boundary radial convergence in the radial velocity field.

b. Convection initiation

The three ingredients required for convection initiation are moisture, instability, and a lifting mechanism (McNulty 1978; Doswell 1987; Johns and Doswell 1992). The relative humidity between the surface and 500 hPa was computed using sounding relative humidity data weighted by the depth of each measurement. The mean relative humidity value between the surface and 500 hPa

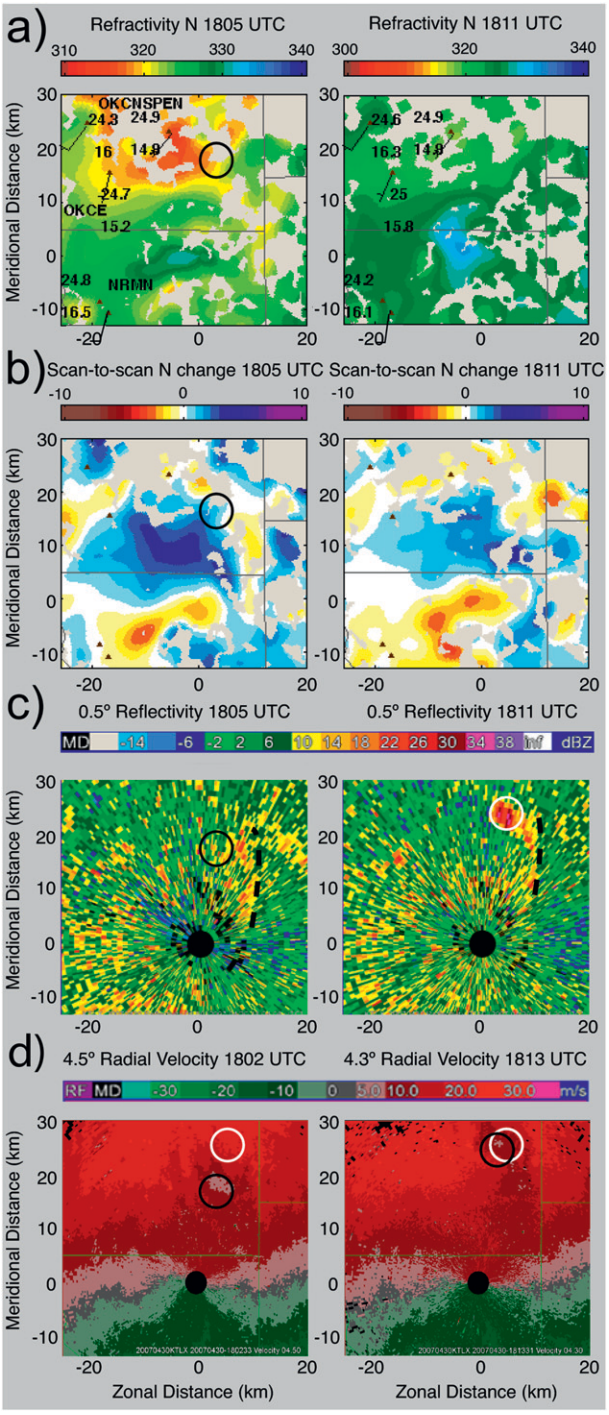

FIG. 5. (a) Refractivity, (b) scan-to-scan refractivity change, (c) 0.5°-tilt reflectivity at 1805 and 1811 UTC 30 Apr 2007, and (d) 4.5° and 4.3°-tilt radial velocity at 1802 and 1813 UTC. In reflectivity, the isolated storm (black circle on each field) was evident just north of the moisture pool at 1811 UTC. The fine line is demarcated by the black dashed line on the reflectivity field. Mesonet temperature, dewpoint temperature, and wind barb (same as Fig. 3) are plotted on the refractivity panels.

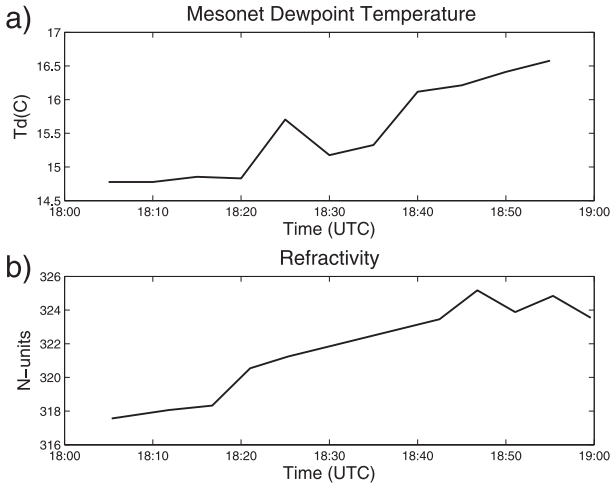

FIG. 6. (a) Time series plot of SPEN dewpoint temperature, and (b) radar refractivity measured at SPEN. The moisture pool passed between 1810 and 1845 UTC, as indicated by an increase in both dewpoint temperature and radar refractivity.

was 72% for the 1200 UTC 30 April 2007 OUN sounding. The moderately high mean relative humidity between the surface and 500 hPa provided sufficient moisture for convection initiation. Approximately 700–800 J kg^{-1} of convective available potential energy (CAPE, shown in forthcoming sounding analysis) provided sufficient instability for convection initiation, and a mesoscale lifting mechanism was evident by the fine line within the MB. While it appears that all three ingredients for convection initiation were available, a LFC of 2385 m and -36 J kg^{-1} of CIN suggested that convection initiation was unlikely without an enhancement in moisture or the low-level lifting mechanism (or both).

Convection initiation using the first 30-dBZ echoes as the threshold (e.g., Wilson and Schreiber 1986) occurred at 1810 UTC at 3.5° elevation. The absence of 30-dBZ reflectivity prior to 1810 UTC can be attributed to insufficient precipitation to produce an enhanced reflectivity structure. However, owing to mass continuity, storm-scale convergence is required to compensate for the developing updraft. Thus, storm-scale convergence can be assumed to be a precursor to the reflectivity-based definition of convection initiation. Since the reflectivity due to ground clutter is significantly higher at lower tilts, the 4.5° tilt was chosen to examine the radial velocity field. At 1811 UTC, storm-scale convergence was nearly collocated with the location of the first 30-dBZ echoes observed at 1810 UTC, as expected from mass continuity (Fig. 5d). The following discussion will discuss the position of the MB, and the developing storm identified by storm-scale convergence, relative to the position of the moisture pool.

TABLE 1. Storm motion and SR flow computed using WDSSII and the average 1745 UTC VAD wind from the two lowest levels.

Times (UTC)	Storm motion (m s^{-1})/direction (°)	SR wind speed (m s^{-1})/direction (°)
1733–1743 UTC	6.4/207	0.8/206
1743–1752 UTC	7.1/189	1.5/290

Prior to 1805 UTC, the position of the MB could not be identified in reflectivity. However, the location of the MB was identified using the radial velocity field and Mesonet data. At 1725 UTC, the winds at the western Mesonet stations (OKCN, OKCE, NRMN) exhibited a westerly component, while the winds at SPEN exhibited an easterly component (Fig. 4a). At 1723 UTC, the maximum inbound velocities near KTLX (within 5 km) were located southeast of the radar (Fig. 4d), implying southeasterly winds in this area. Thus, these observations reveal convergent flow between the western Mesonet stations and the region near SPEN and KTLX, which suggests that the MB was located west of KTLX and SPEN. Between 1723 and 1745 UTC, the wind direction at SPEN shifted from 160° to 190°, and the maximum inbound velocities near KTLX shifted from about 150° to 190°. The wind shift observed at KTLX and SPEN implies the movement of the MB from west to east. Thus, the MB was likely just east of the SPEN station at 1745 UTC, and therefore provided a mesoscale lifting mechanism in the vicinity of the ensuing convection initiation.

To determine the position of the developing storm prior to first echoes, storm-scale convergence was identified in the radial velocity field. Storm-scale convergence can be seen in the 4.5°-tilt radial velocity fields at 1733, 1743, and 1752 UTC (Fig. 4d) and at 1802 and 1813 UTC (Fig. 5d). The average computed storm-scale convergence values (over 10–12 radially adjacent gates along convergence axis) ranged between 0.003 to 0.004 s^{-1} between 1733 and 1752 UTC. The northward movement of the storm-scale convergence between 1733 and 1813 UTC is consistent with the northerly storm motion (Table 1). These observations imply the presence of an updraft associated with the developing storm as early as 1733 UTC. Given that the first 30-dBZ echoes occurred about 30 min later, and storm-scale convergence was not observed prior to 1733 UTC, the initial updraft likely reached the LFC around 1733 UTC.

For at least 45 min prior to convection initiation, the MB and storm-scale convergence associated with the developing storm resided within the moisture pool. At 1726 UTC, the moisture pool was also located within the area of convergence associated with the MB (Fig. 4). The MB provided a lifting mechanism to support the development of a deep, convective updraft within the

moisture pool. The moisture pool and convergent signature were also closest at the earliest observation of storm-scale convergence (Fig. 4). The storm-scale convergence associated with the developing storm was located on the northeast side of the moisture pool at 1736, 1745, 1755, and 1805 UTC (Figs. 4 and 5), showing that the developing storm resided in a region with higher surface moisture for 35 min prior to convection initiation at 1811 UTC. At 1755 and 1805 UTC, even though the storm began to move into drier air to the north, increasing moisture was still observed in scan-to-scan refractivity and refractivity values remained higher than those observed at SPEN and OKCE (Figs. 4 and 5).

To determine if the developing storm ingested the higher surface moisture, the near-surface storm-relative (SR) wind was computed using VAD data and storm motion acquired from WDSSII. The average 1745 UTC VAD wind speed and direction at the lowest two levels (38 and 129 m) were 7.2 m s^{-1} and 201°, respectively, very close to the storm motion. The magnitudes of near-surface SR wind were thus very small (Table 1), indicating that the storm was ingesting the higher moisture very close to the storm during convection initiation. Assuming a 2 m s^{-1} updraft and a LFC height of 1833 m within the moisture pool, moist surface air would reach the LFC in 15.3 min. Thus, the 45-min residency time of the moisture pool near the MB and during convection initiation was sufficient for the moist air to reach the LFC. The next section investigates the impact of ingesting the higher moisture on convection initiation.

c. *Impact of moisture variability on convection initiation*

To assess the impact of moisture variability on convection initiation, NSHARP (Hart and Korotky 1991) was used to modify soundings. Several upper-air observations were considered for the sounding analysis because upper-air observations were unavailable at the time and location of convection initiation. An 1800 UTC LMT sounding provided the most timely upper-air measurement, but was located 180 km from the convection initiation region. The closest soundings to the convection initiation region were the 1200 UTC 30 April 2007 and 0000 UTC 1 May 2007 OUN soundings. The 1700 and 1900 UTC RUC soundings were also available near the region of convection initiation. However, the surface and boundary layer moisture values in the RUC soundings were too high compared to surface and upper-air observations, and the vertical resolution (50 hPa) was limited compared to the upper-air observations. From these data sources, the 1200 UTC 30 April 2007 sounding was selected for further analysis given its spatial proximity to convection initiation.

TABLE 2. Thermodynamic variables from the 1200 UTC 30 Apr 2007 OUN sounding analyses.

Case	T (°C)	T_d (°C)	CIN (J kg^{-1})	CAPE (J kg^{-1})	LFC (m)	LCL (m)
Scenario 1	25	15	−36	745	2385	1345
Scenario 2	25	16.4	−12	1389	2080	1170
Scenario 3	25	17	−3	1717	1833	1094

When performing a sounding analysis, there is no standard method for determining the initial parcel temperature and mixing ratio (Doswell and Rasmussen 1994). Commonly, the initial parcel temperature and mixing ratio are determined from surface observations, mean values through a specified depth, or a parcel with the largest CAPE (Doswell and Rasmussen 1994). For this study, surface observations are considered most appropriate because timely upper-air observations were unavailable. For this study, it is assumed that the Mesonet and refractivity observations are representative of a parcel mixed throughout the boundary layer. As discussed previously, the moisture pool was collocated with the MB and developing storm for at least 45 min prior to convection initiation, allowing sufficient mixing time through the boundary layer. Owing to the absence of updated boundary layer moisture data, this study cannot account for the vertical mixing of moisture throughout the boundary layer. Based on these assumptions, the sounding analysis was conducted using the average Mesonet surface temperature closest to the region of convection initiation (OKCE and SPEN). Using this surface temperature, the boundary layer temperature profile was modified to well-mixed conditions through 875 hPa, based on a 900-hPa mixed layer height seen in the 1700 UTC RUC sounding, and assuming a slight increase in mixing layer height after an additional hour of boundary layer mixing.

Three scenarios were created to investigate the impact of moisture variability on convection initiation. Scenario 1 was based on the average surface temperature and dewpoint temperature from the Mesonet stations closest to the region of convection initiation (OKCE and SPEN) prior to convection initiation. Scenario 2 examined a 1.4°C dewpoint temperature increase based on the SPEN Mesonet dewpoint temperature change caused by the moisture pool. Scenario 3 investigated a 2°C increase in dewpoint temperature based on the observed radar refractivity difference across the moisture pool. The modified 1200 UTC OUN sounding was further modified based on scenarios 1–3 to create three new soundings, using the surface conditions listed in Table 2. In Fig. 7, the modified 1200 UTC sounding for scenario 1 is shown.

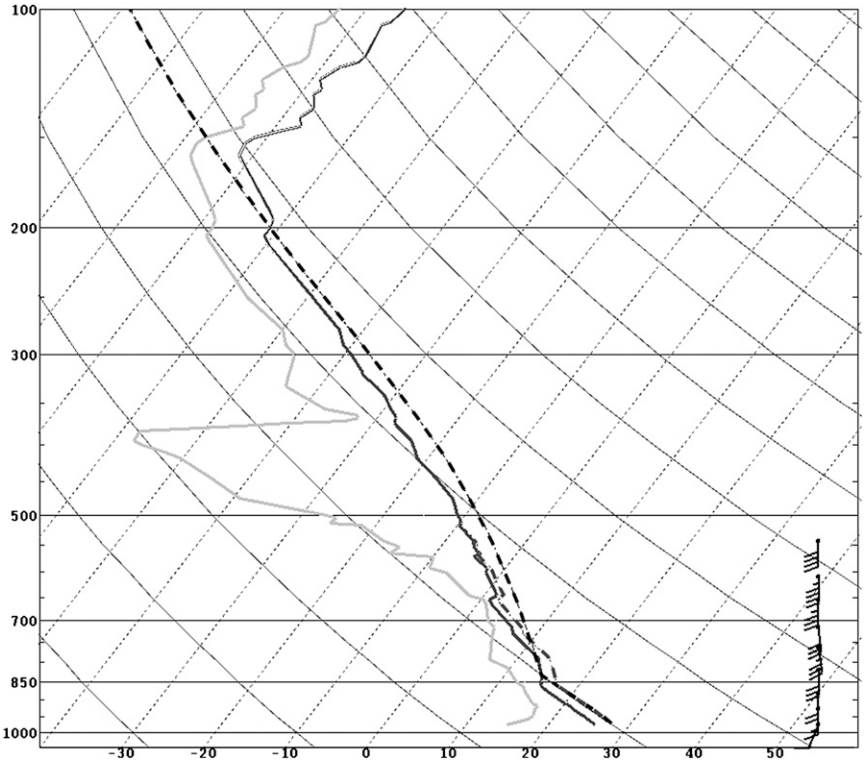

FIG. 7. The 1200 UTC OUN sounding modified for scenario 1 ($T = 25$°C and $T_d = 15$°C). The dewpoint temperature (solid light gray line), and temperature (solid dark gray line) profiles are plotted on the sounding. The dashed dark gray line indicates the modified environmental temperature, and the dashed black line indicates the parcel temperature. The 1745 VAD wind profile is plotted using wind barbs (barb values are the same as Fig. 3).

The modified sounding for scenario 1 (Fig. 8a) showed CIN of -36 J kg^{-1} and a high LFC of 2385 m (Table 2). This CIN value would require an 8.5 m s^{-1} updraft to overcome the stable layer and reach the LFC. This updraft velocity is higher than updraft velocities typically observed in the boundary layer, even within the most intense convective updrafts in convergence zones. For example, Parsons et al. (1991) and Ziegler et al. (1997) found that the maximum velocities in boundary layer updrafts in drylines were about 5 m s^{-1}. Miao et al. (2006) and Geerts and Miao (2005) presented observations where the maximum boundary layer vertical velocities were generally 2–4 m s^{-1}. Other studies have found that CIN must decrease below a certain threshold for convection initiation. Weckwerth (2000) showed that convection initiation cases commonly occurred when CIN was near zero. In a modeling study of convection initiation, Colby (1984) presented a case where the absolute value of CIN needed to decrease below 16 J kg^{-1} before deep convection commenced. Based on these studies and the computed CIN, convection initiation was unlikely under these thermodynamic conditions without further changes in stability or substantial low-level lifting.

Scenarios 2 and 3 investigate the possibility that enhanced moisture within the moisture pool produced a more favorable thermodynamic environment for convection initiation (Table 2). Based on the Mesonet-observed moisture increase associated with the moisture pool (scenario 2), the moisture pool reduced CIN from -36 to -12 J kg^{-1} and the height of the LFC was reduced from 2385 to 2080 m (Fig. 8b). Considering the increase in moisture from the refractivity-based moisture observations (scenario 3), the LFC was reduced from 2385 to 1833 m and CIN was reduced to near zero (Fig. 8c). In scenario 2, a 4.9 m s^{-1} updraft would be required to overcome the residual CIN. Based on the maximum updrafts observed by Parsons et al. (1991) and Ziegler et al. (1997), this updraft magnitude is only common among the strongest updrafts within convergence zones. In scenario 3, CIN is nearly expunged and a convective updraft of just 2.4 m s^{-1} would be required to overcome the residual stable layer. The near-zero CIN is consistent with CIN values observed by Weckwerth (2000) and Colby (1984) in convection initiation cases, and the updraft velocity required to overcome CIN is within the range of updraft velocities observed in the boundary

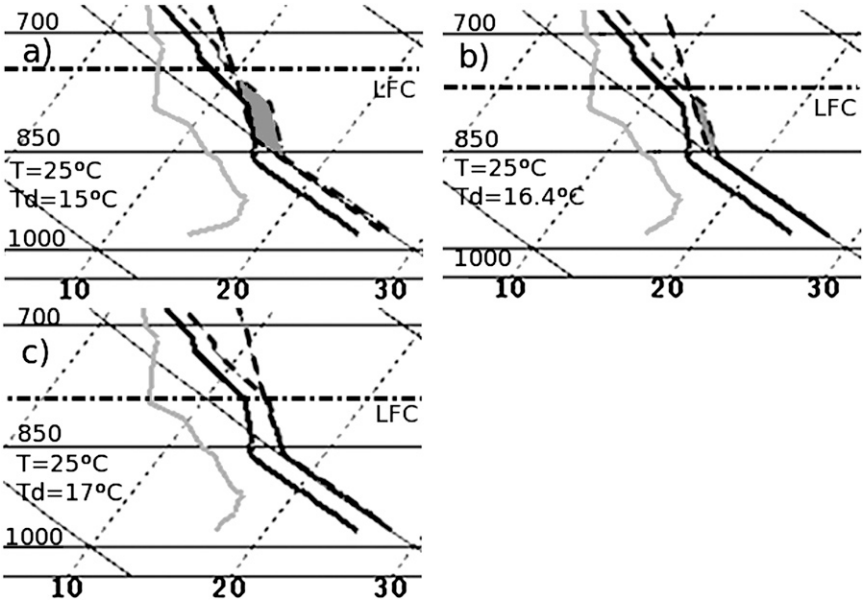

FIG. 8. The 1200 UTC OUN sounding, further modified to simulate the impact of moisture variability near the convection initiation region. (a)–(c) Soundings correspond to scenarios 1–3, where (a) $T = 25$°C and $T_d = 15$°C, (b) $T = 25$°C and $T_d = 16.4$°C, and (c) $T = 25$°C and $T_d = 17$°C. The temperature, dewpoint temperature, modified environmental temperature, and parcel temperature are the same as Fig. 7. The shaded area delineates the area of CIN, and the LFC is annotated with a dashed–dotted black line.

layer and convergence zones. Moreover, the LFC is reduced by about 500 m, reducing the distance required for a convective updraft to become positively buoyant. CAPE for scenario 3 was 2.5 times higher than scenario 1, indicating that the instability was significantly greater within the moisture pool.

Based on the results from scenario 3, the moisture pool created a much more favorable environment for convection initiation with near-zero CIN, a lower LFC, and much higher instability. Thus, the potential for convection initiation was much higher within the moisture pool compared to the surrounding environment. We believe that the results from scenario 3 are more representative of the convection initiation region because the moisture measurements were located within the region of convection initiation whereas the Mesonet measurements were 25 km from the region of convection initiation. Additionally, the moisture pool passed over SPEN after convection initiation occurred.

5. Conclusions

The 30 April 2007 case was used to examine the effects of moisture variability on convection initiation in a synoptically active environment, using radar refractivity retrievals to reanalyze soundings. Although the three ingredients for convection initiation were nearly sufficient, -36 J kg^{-1} of CIN and a high LFC suggested that convection initiation was unlikely. Thus, an enhancement in moisture or lift was necessary for convection initiation. Radar refractivity data showed relatively high small-scale moisture variability associated with a moisture pool. Radial velocity and Mesonet data revealed that the MB and developing storm were collocated with the moisture pool for at least 45 min prior to convection initiation, and the developing storm ingested the higher moisture associated with the moisture pool. NSHARP was used to modify soundings to investigate the impact of moisture variability on convection initiation. The modified soundings showed that the higher moisture within the moisture pool increased the potential for convection initiation by producing a more favorable thermodynamic environment with near-zero CIN, a lower LFC, and much higher CAPE.

Unlike previous studies, the 30 April 2007 case revealed observational evidence that moisture variability in a synoptically active environment impacted convection initiation in the absence of boundaries with strong moisture gradients (e.g., dryline, outflow boundary). Moreover, this study investigated the new application of using radar refractivity data to examine the thermodynamic impact of small-scale moisture variability. This study corroborates observational results from Weckwerth (2000), which found that moisture variability significantly

increased the likelihood of convection initiation within regions of higher moisture by reducing CIN, lowering the LFC, and increasing CAPE. This study showed that convection initiation was only supported thermodynamically within a local maximum in the moisture field. Our study also supports the work of Fabry (2006) by illustrating a case where the effects of moisture variability on convection initiation were greatest at scales less than 20 km. The moisture pool observed in refractivity and scan-to-scan refractivity possessed a wavelength of about 15–20 km, so moisture variability at scales less than 20 km was critical for this case. The higher sensitivity of observed moisture variability to temperature variability in this case differs from the results presented in Crook (1996), most likely because the temperature variability was much lower than the moisture variability.

The reduction of CIN, to a value that can be overcome by convective updrafts, is a necessary, but insufficient condition for convection initiation. Thus, while refractivity data exhibited utility for examining if CIN can be reduced sufficiently, the development of the storm with reduced CIN depends on conditions that affect deep convection (e.g., instability, entrainment). Hence, for convection initiation, the primary utility for refractivity data may be assessing changes in CIN based on the observed moisture variability. Inferring the variability of CAPE based on moisture variability observed by refractivity data could potentially improve estimates of updraft strength and the likelihood of deep convection. In this study, the storm resided in a region of higher moisture, which may explain why an intense storm developed after ingesting the higher moisture for at least 45 min prior to convection initiation.

The case study illustrated the capability of radar refractivity data to resolve moisture variability at smaller scales than the available surface moisture measurements. Refractivity data showed that significant moisture variability can occur between Mesonet stations, suggesting that refractivity data could be a useful surrogate data source for observing small-scale moisture variability. Although the Mesonet data showed an increase in moisture associated with the moisture pool, the spatial extent of the moisture pool was poorly resolved compared to the radar refractivity data, which clearly demarcated the spatial structure of the moisture pool. An examination of refractivity data revealed that the moisture pool and initial storm updraft were collocated; this association between these features could only be speculated on using the nearest surface station. Although there is a growing impetus for higher resolution surface mesonets, few states have a good surrogate surface network to the ASOS network. The results from this study and previous studies (e.g., Heinselman et al. 2009) suggest that refractivity data would have even greater utility in locations without mesonets, because the typical refractivity domain (about 80-km wide) will only have one ASOS station, based on the 90-km average spacing of ASOS stations.

Acknowledgments. Funding for this research was provided by the Radar Operations Center through grant number NA17RJ1227 and the National Science Foundation through Grant ATM0750790. The first author was supported by an American Meteorological Society Fellowship sponsored by the Raytheon Corporation. This manuscript benefited from reviews and discussions with Conrad Ziegler and Rodger Brown, and reviews from two anonymous reviewers. The authors thank the Radar Operations Center for maintaining the data flow from KTLX during the experiment. The authors also thank Mark Laufersweiler, Kevin Manross, and Travis Smith for their assistance with data acquisition and computing support.

REFERENCES

Bean, B. R., and E. J. Dutton, 1968: *Radio Meteorology*. Dover Publications, 435 pp.

Benjamin, S. G., and Coauthors, 2004: An hourly assimilation/forecast cycle: The RUC. *Mon. Wea. Rev.,* **132,** 495–518.

Brock, F. V., K. C. Crawford, R. L. Elliott, G. W. Cuperus, S. J. Stadler, H. L. Johnson, and M. D. Eilts, 1995: The Oklahoma Mesonet: A technical overview. *J. Atmos. Oceanic Technol.,* **12,** 5–19.

Buban, M. S., C. L. Ziegler, E. N. Rasmussen, and Y. P. Richardson, 2007: The dryline on 22 May 2002 during IHOP: Ground-radar and in situ data analyses of the dryline and boundary layer evolution. *Mon. Wea. Rev.,* **135,** 2473–2505.

Cheong, B. L., R. D. Palmer, C. D. Curtis, T.-Y. Yu, D. S. Zrnić, and D. Forsyth, 2008: Refractivity retrieval using the Phased Array Radar: First results and potential for multi-function operation. *IEEE Trans. Geosci. Remote Sens.,* **46,** 2527–2537.

Colby, F. P., 1984: Convective inhibition as a predictor of convection during AVE-SESAME II. *Mon. Wea. Rev.,* **112,** 2239–2252.

Crook, N. A., 1996: Sensitivity of moist convection forced by boundary layer processes to low-level thermodynamic fields. *Mon. Wea. Rev.,* **124,** 1767–1785.

Dabberdt, W. F., and T. W. Schlatter, 1996: Research opportunities from emerging atmospheric observing and modeling capabilities. *Bull. Amer. Meteor. Soc.,* **77,** 305–323.

Demoz, B., and Coauthors, 2006: The dryline on 22 May 2002 during IHOP: Convective-scale measurements at the profiling site. *Mon. Wea. Rev.,* **134,** 294–310.

Doswell, C. A., 1987: The distinction between large-scale and mesoscale contribution to severe convection: A case study example. *Wea. Forecasting,* **2,** 3–16.

——, and E. N. Rasmussen, 1994: The effect of neglecting the virtual temperature correction on CAPE calculations. *Wea. Forecasting,* **9,** 625–629.

Emanuel, K., and Coauthors, 1995: Report of first prospectus development team of the U.S. Weather Research Program to NOAA and the NSF. *Bull. Amer. Meteor. Soc.,* **76,** 1194–1208.

Fabry, F., 2004: Meteorological value of ground target measurements by radar. *J. Atmos. Oceanic Technol.,* **21,** 560–573.

——, 2006: The spatial variability of moisture in the boundary layer and its effect on convective initiation: Project-long characterization. *Mon. Wea. Rev.,* **134,** 79–91.

——, C. Frush, I. Zawadzki, and A. Kilambi, 1997: On the extraction of near-surface index of refraction using radar phase measurements from ground targets. *J. Atmos. Oceanic Technol.,* **14,** 978–987.

Geerts, B., and Q. Miao, 2005: The use of millimeter Doppler radar echoes to estimate vertical air velocities in fair-weather convective boundary layer. *J. Atmos. Oceanic Technol.,* **22,** 225–246.

Hart, J. A., and W. Korotky, 1991: The sharp workstation vl.50 users guide. NOAA/National Weather Service Tech Rep., 30 pp.

Heinselman, P. L., B. L. Cheong, R. D. Palmer, D. Bodine, and K. Hondl, 2009: Radar refractivity retrievals in Oklahoma: Insights into operational benefits and limitations. *Wea. Forecasting,* **24,** 1345–1361.

Johns, R. H., and C. A. Doswell, 1992: Severe local storms forecasting. *Wea. Forecasting,* **7,** 588–612.

Koch, S. E., and S. Saleeby, 2001: An automated system for the analysis of gravity waves and other mesoscale phenomena. *Wea. Forecasting,* **16,** 661–679.

Lakshmanan, V., T. Smith, K. Hondl, G. J. Stumpf, and A. Witt, 2006: A real-time, three-dimensional, rapidly updating, heterogeneous radar merger technique for reflectivity, velocity, and derived products. *Wea. Forecasting,* **21,** 802–823.

——, ——, G. J. Stumpf, and K. Hondl, 2007: The Warning Decision Support System–Integrated Information. *Wea. Forecasting,* **22,** 596–612.

McLaughlin, D., and Coauthors, 2009: Short-wavelength technology and the potential for distributed networks of small radar systems. *Bull. Amer. Meteor. Soc.,* **90,** 1797–1817.

McNulty, R. P., 1978: On upper tropospheric kinematics and severe weather occurrence. *Mon. Wea. Rev.,* **106,** 662–672.

McPherson, R. A., and Coauthors, 2007: Statewide monitoring of the mesoscale environment: A technical update on the Oklahoma Mesonet. *J. Atmos. Oceanic Technol.,* **24,** 301–321.

Miao, Q., B. Geerts, and M. LeMone, 2006: Vertical velocity and buoyancy characteristics of coherent echo plumes in the convective boundary layer, detected by a profiling airborne radar. *J. Appl. Meteor. Climatol.,* **45,** 838–855.

National Research Council, 1998: *The Atmospheric Sciences: Entering the Twenty-First Century*. National Academy Press, 373 pp.

Parsons, D. B., M. A. Shapiro, R. M. Hardesty, R. J. Zamora, and J. M. Intrieri, 1991: The finescale structure of a west Texas dryline. *Mon. Wea. Rev.,* **119,** 1242–1258.

——, ——, and E. Miller, 2000: The mesoscale structure of a nocturnal dryline and of a frontal-dryline merger. *Mon. Wea. Rev.,* **128,** 3824–3838.

Roberts, R. D., and Coauthors, 2008: REFRACTT-2006: Real-time retrieval of high-resolution low-level moisture fields from operational NEXRAD and research radars. *Bull. Amer. Meteor. Soc.,* **89,** 1535–1548.

Wakimoto, R. M., and H. V. Murphey, 2009: Analysis of a dryline during IHOP: Implications for convection initiation. *Mon. Wea. Rev.,* **137,** 912–936.

Weckwerth, T. M., 2000: The effect of small-scale moisture variability on thunderstorm initiation. *Mon. Wea. Rev.,* **128,** 4017–4030.

——, J. W. Wilson, and R. M. Wakimoto, 1996: Thermodynamic variability within the convective boundary layer due to horizontal convective rolls. *Mon. Wea. Rev.,* **124,** 769–784.

——, and Coauthors, 2004: An overview of the International H20 Project (IHOP) and some preliminary highlights. *Bull. Amer. Meteor. Soc.,* **85,** 253–277.

——, C. R. Pettet, F. Fabry, S. Park, M. A. LeMone, and J. W. Wilson, 2005: Radar refractivity retrieval: Validation and application to short-term forecasting. *J. Appl. Meteor.,* **44,** 285–300.

Wilson, J. W., and W. E. Schreiber, 1986: Initiation of convective storms at radar-observed boundary-layer convergence lines. *Mon. Wea. Rev.,* **114,** 2516–2536.

Ziegler, C. L., and E. N. Rasmussen, 1998: The initiation of moist convection at the dryline: Forecasting issues from a case study perspective. *Wea. Forecasting,* **13,** 1106–1131.

——, T. J. Lee, and R. A. Pielke, 1997: Convective initiation at the dryline: A modeling study. *Mon. Wea. Rev.,* **125,** 1001–1026.

Zrnić, D. S., and Coauthors, 2007: Agile-beam phased array radar for weather observations. *Bull. Amer. Meteor. Soc.,* **88,** 1753–1766.